

Article

# Propagation Characteristics of Modulated EHF Signal in the Wake Region of Plasma Sheath

Xiaocui Yang<sup>1,2</sup>, Kai Yuan<sup>3</sup>, Yuhao Wang<sup>3,4,\*</sup>, Yiwen Liu<sup>3</sup> and Jiawei Xiong<sup>3</sup>

<sup>1</sup> Key Laboratory of Poyang Lake Environment and Resource Utilization, Ministry of Education, School of Resources Environmental Chemical Engineering, Nanchang University, Nanchang 330031, China; yxczcl@163.com

<sup>2</sup> Institute of Space Science and Technology, Nanchang University, Nanchang 330031, China

<sup>3</sup> School of Information Engineering, Nanchang University, Nanchang 330031, China; yuankai@ncu.edu.cn (K.Y.); liuyiwen@whu.edu.cn (Y.L.); jiaweixiong\_ncu@163.com (J.X.)

<sup>4</sup> School of Physics and Electronic Information, Shangrao Normal University, Shangrao 334001, China

\* Correspondence: wangyuhao@ncu.edu.cn

**Abstract:** A large number of studies have confirmed that the wake region may be a more ideal antenna installation area for the reentry vehicle communication problem, but many practical issues such as how to choose the modulation mode, carrier frequency, and antenna orientation are still pending. Based on numerical simulations, the characteristics of tail channels and the bit error rate (BER) of extremely high-frequency (EHF) communication in the wake region of the plasma sheath of hypersonic vehicle are studied. It is found that, with an increase in the angle between the tail channel and the tail of the vehicle, the attenuation of the EHF signals decreases and the phase shift fluctuates more severely. In order to obtain better communication performance, 2PSK with a carrier frequency of 140 GHz or 225 GHz, or 4QAM (QPSK) modulation with a carrier frequency of 140 GHz, and the tail channel with an angle between 50° and 60° to the tail of the vehicle can be selected. This study reveals the propagation characteristics and BER performance of EHF signals in the wake region of plasma sheath, which can provide a valuable reference for the design of the hypersonic vehicle communication system.

**Keywords:** plasma sheath; wake; modulated EHF signal; SMM; antenna location



**Citation:** Yang, X.; Yuan, K.; Wang, Y.; Liu, Y.; Xiong, J. Propagation Characteristics of Modulated EHF Signal in the Wake Region of Plasma Sheath. *Aerospace* **2022**, *9*, 194. <https://doi.org/10.3390/aerospace9040194>

Academic Editor: Gokhan Inalhan

Received: 15 February 2022

Accepted: 1 April 2022

Published: 4 April 2022

**Publisher's Note:** MDPI stays neutral with regard to jurisdictional claims in published maps and institutional affiliations.



**Copyright:** © 2022 by the authors. Licensee MDPI, Basel, Switzerland. This article is an open access article distributed under the terms and conditions of the Creative Commons Attribution (CC BY) license (<https://creativecommons.org/licenses/by/4.0/>).

## 1. Introduction

A plasma sheath is formed around a vehicle when it re-enters Earth's atmosphere at hypersonic speeds, resulting in the loss or weakening of the communication signal, forming the so-called "blackout" phenomenon [1,2]. In the past few decades, a large number of theoretical and experimental studies have been carried out to mitigate the influence of the communication "blackout". The most promising technologies to solve the "blackout" problem include injecting electrophilic substances from the antenna location upstream of the plasma flow field and changing the plasma flow field by aerodynamic forming [3,4]. However, the above methods are still very difficult to universally implement in engineering. For instance, aerodynamic forming needs to change the shape of the vehicle, which might limit the available volume of the vehicle. The electrophilic material injection would reduce the mission payloads of the vehicle. Therefore, some alternatives have been proposed, such as high-frequency communication and proper antenna locations [5–8]. In recent years, great progress in high-frequency signal sources and antennas has provided great opportunities for high-frequency communication solutions [9,10]. A large number of studies showed that the extremely high-frequency (EHF) wave is higher than the cutoff frequency of plasma sheaths, i.e., it is feasible to mitigate the communication blackout with EHF communication [11–13].

Some groups have studied the propagation characteristics of an EHF wave in inhomogeneous colliding magnetic plasma [14], non-magnetic plasma [12,15–17], high-temperature, non-magnetic plasma sheath [18], and realistic plasma sheath [11–13] from many aspects. Tang et al. found that the total attenuation of an EHF signal is affected by the plasma distribution structure on the signal transmission path [19]. Moreover, the spatiotemporal characteristics of plasma sheath have also been widely studied. The results showed that the spatial distribution of plasma sheath is inhomogeneous and time-varying [20–23].

In addition, the installation positions of the communication antenna has been a matter of concern in the recent decade. Among them, the wall and the nose of the vehicle were studied earlier and more comprehensively, because the direct communication link between ground station and vehicle is usually considered. The antennas for RAM C-I and RAM C-II flight tests are installed near the nose and on the wall of the vehicles, respectively [1]. Belov et al. showed that installing a remote antenna module in a dedicated small container on top of the vehicle can provide uninterrupted radio communication with the reentry vehicle, although there are many problems related to the heating and thermal protection of vessels and towers [6]. On the other hand, some research studies have revealed that installing the antenna on the wall close to the tail is helpful for mitigating the “blackout” for a blunt-coned reentry vehicle [11,24]. In those works, the communication signals are usually supposed to penetrate the plasma sheath via the aft region, which is near the wall and close to the tail of the vehicle. In other words, the channel is supposed to be in the aft region in those works.

On the other hand, the wake region has also been suggested to possess potential channels by some researchers. The wake region was investigated by scientists and engineers soon after the blackout was discovered in 1950s [25]. In 1960s, the US launched the FIRE project, which partly aimed at investigating the flow field of the wake region of reentry plasma sheaths [26]. Since then, researchers have studied the evolution of the structure of wake regions and its mechanics. According to previous work, although the energy loss of propagating signals could occur due to the scattering caused by turbulences in wake regions [27], the electron densities in the wake region of blunt-coned plasma sheaths are lower than that in the aft region [28,29]. High-frequency signals could penetrate the plasma sheath via wake regions with less signal attenuation compared with other regions of plasma sheaths [30].

In order to make the signals propagate in the wake region, the onboard antenna needs to be installed at the tail of the vehicle. Since the electron density of the tail is the lowest during the evolution of the sheath, the performance of communication via wake region may be better than that via aft region, particularly when relay communication is adopted [31,32]. The Atmospheric Reentry Demonstrator (ARD) experiment used NASA’s Tracking and Data Relay Satellite (TDRS) for communication. During the experiment, the duration of “blackout” was much shorter than was expected. Theoretical analysis shows that the shorter “blackout” might be attributed to the lower electron density in the wake region [33].

In general, the existing works showed that the wake region has less signal attenuation and that the wake region may be a more ideal antenna installation area. However, it should be noted that “blackout” is a communication problem, and many factors may have an important impact on the communication performance, such as signal modulation mode, carrier frequency selection, and antenna orientation. However, so far, there is still a lack of research on these issues. In other words, if the antenna is installed in the wake area, there is a very important and practical issue that is not clear, that is: what is the optimal comprehensive design scheme of the modulation mode, carrier frequency, and antenna direction?

In this paper, the communication performance of modulated EHF signals with different modulation modes in different channels in the wake region of a blunt-coned plasma sheath are studied. It aimed to propose the optimal combination design scheme for the modulation mode and the carrier frequency, as well as the optimal channel angle design scheme. The

results are helpful in solving the “blackout” problem that occurs when relay communication is adopted in engineering.

## 2. Characteristics of EHF Wave in Plasma Sheath

### 2.1. Analysis Method

In this paper, the propagation characteristics of EHF signals in the plasma sheath of a blunt-coned hypersonic vehicle were studied using a one-dimensional plate model. The plasma sheath model used here was the same as in the article [11]. For the shape and the size of the spacecraft, we adopted the parameters of the spacecraft in the RAM C-II experiment; that is, the radius of the sphere in the front of the aircraft is 15.24 cm, the half angle of the cone is  $9^\circ$ , and the length is 1.295 m. RAM series flight experiments are one of the most important experiments with which to study the “black out” problem in the history of aerospace. The parameters and data of RAM C-I and RAM C-II experiments have been published for a long time and are frequently cited [1,34]. The flying altitude of the spacecraft was set to 31 km, which is the most serious altitude of “blackout” in an RAM C-II test [13]. The flight speed was set to 6550 m/s, which was the same as that of RAM C-II reentry vehicle, at an altitude of 31 km. In addition, the plasma sheath is obviously influenced by the atmospheric conditions around the hypersonic vehicle. The atmospheric condition used in this paper was obtained from the NRLMSISE00 model, which is an empirical atmospheric model available online. In addition, for the antenna location, because there will be turbulent structures near the center of the wake or the edge of the bottom, which will seriously affect the communication stability, the antenna can only be placed between the wake center and the edge of the bottom. For the channel angle, if the inclination angle is too large, an increase in the transmission path will cause strong total signal attenuation, and if the inclination angle is too small, there will be large polarization loss on the antenna. Therefore, the selected channel angle must also be moderate. In general, the selection of the simulation parameters is used to obtain the optimal communication scheme.

It is assumed that the antenna is installed at the tail of vehicle (see point A in Figure 1) and that the signal path is inclined outward. Point B represents the side signal incidence position. Figure 1 shows only half of the plasma sheath since the angle of attack is set to  $0^\circ$  and the plasma sheath is symmetrical. The symmetry axis of the vehicle is selected as the X axis and the vehicle vertex coordinates and antenna coordinates are set to (0, 0) and (−1.295, 0.27), respectively. The half cone angle of the blunt cone hypersonic vehicle is  $9^\circ$ . The color axis represents the electron density. In Figure 1b, the channels in the wake region of the plasma sheath are identified as 1–6, respectively. The angles between channels 1 and 6 and the tail of the vehicle are:  $32^\circ$ ,  $36^\circ$ ,  $44^\circ$ ,  $48^\circ$ ,  $56^\circ$ , and  $58^\circ$ , respectively. The propagation characteristic parameters are obtained by the following method.

First of all, it should be noted that it is very difficult to determine the optimal incidence angle because the signal can only adopt oblique incidence in tail communication. Here, we used the refraction law under approximate conditions to determine the incident angle before carrying out scattering matrix method (SMM) analysis. Assuming that the signal propagation path between point A and point B is a straight line, the refraction angle  $\gamma$  on the sheath boundary will be approximately  $9^\circ$  (half cone angle of the blunt cone hypersonic vehicle) greater than angle  $\alpha$  (angle between the channel and the tail of the vehicle). Then, the incident angle  $\beta$  on the sheath boundary can be deduced from the angle  $\gamma$  by using the refraction law. Moreover, the incident angle  $\theta_i$  in the SMM calculation coordinate system can be obtained by Formula (1).

$$\theta_i = \beta - \gamma \quad (1)$$

Then, based on the SMM [13,20,35], the plasma plate between point A and point B is divided into  $n$  homogeneous thin layers (see red parallel lines in Figure 1a). The propagation characteristic parameters of waves in the whole plasma medium, such as

transmission, reflection, and absorption, can be obtained by a global scattering matrix, which is expressed as:

$$s_g = s_1 s_2 s_3 \dots s_{n-2} s_{n-1} s_n = \prod_{m=1}^n s_m \tag{2}$$

where  $s_m$  is the scattering matrix of the  $m$ -th sublayer, which can be derived from the wave number  $k(m)$  at the  $m$ -th sublayer. Then, using the interface condition of the bottom boundary electromagnetic field in Figure 1, we can obtain:

$$s_g \begin{bmatrix} R \\ 1 \end{bmatrix} = \frac{1}{2k_x^{(n)}} \begin{bmatrix} a_1 e^{ib_1 d_{n+1}} \\ b_1 e^{-ia_1 d_{n+1}} \end{bmatrix} \cdot T \tag{3}$$

where  $a_1 = k_x^{(n)} + k_x^{(n+1)}$ ,  $b_1 = k_x^{(n)} - k_x^{(n+1)}$ ,  $R$  and  $T$  are the global reflection coefficient and global transmission coefficient, respectively. The superscript  $n + 1$  denotes the region III. Finally, the signal transmission rate can be expressed as:

$$T' = T \cdot \sin \alpha \tag{4}$$

Note that  $T'$  is a complex number, and that the amplitude and the phase of  $T'$  represent the transmission coefficient and the phase shift, respectively.

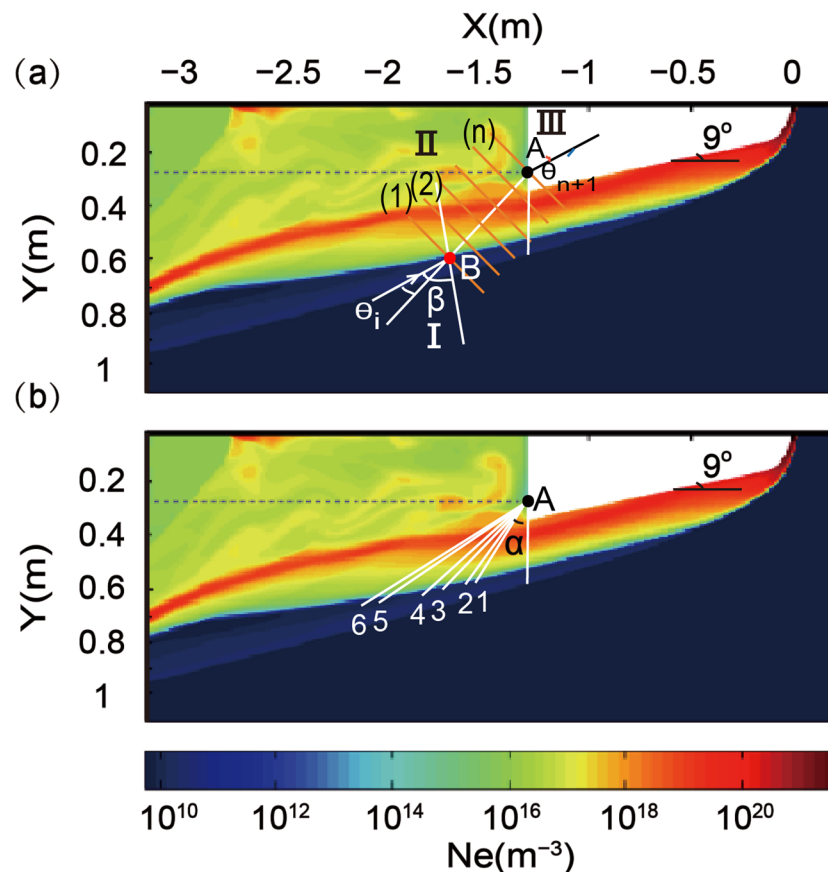


**Figure 1.** (a) Schematic diagram of stratified propagation of oblique incident plane wave at the tail of plasma sheath and (b) signal transmission channels at the tail of plasma sheath.

2.2. Spatiotemporal Evolution Characteristics of EHF Wave in the Wake Region of Plasma Sheath

Figure 2 shows the time-varying curves of the total transmission coefficient (top panels) and phase shift (bottom panels) of EHF signals with carrier frequencies of 94 GHz, 140 GHz, and 225 GHz in the tail channels 1–6. Note that the time resolution of the curves in Figure 2

is  $10^{-5}$  s, and that the transmission coefficient and phase shift at each time point are obtained by Equation (4). Figure 2 reveals that, for a specific carrier frequency, the greater the angle between the channel and the tail of the vehicle, the greater the transmission coefficient. For example, for the carrier frequency of 94 GHz, the total transmission coefficient increases significantly from an average of about 0.45 at an angle of  $36^\circ$  (channel 1) to an average of about 0.78 at  $58^\circ$  (channel 6). The increase in the total transmission coefficients from channel 1 to channel 6 is mainly due to the polarization loss [13].

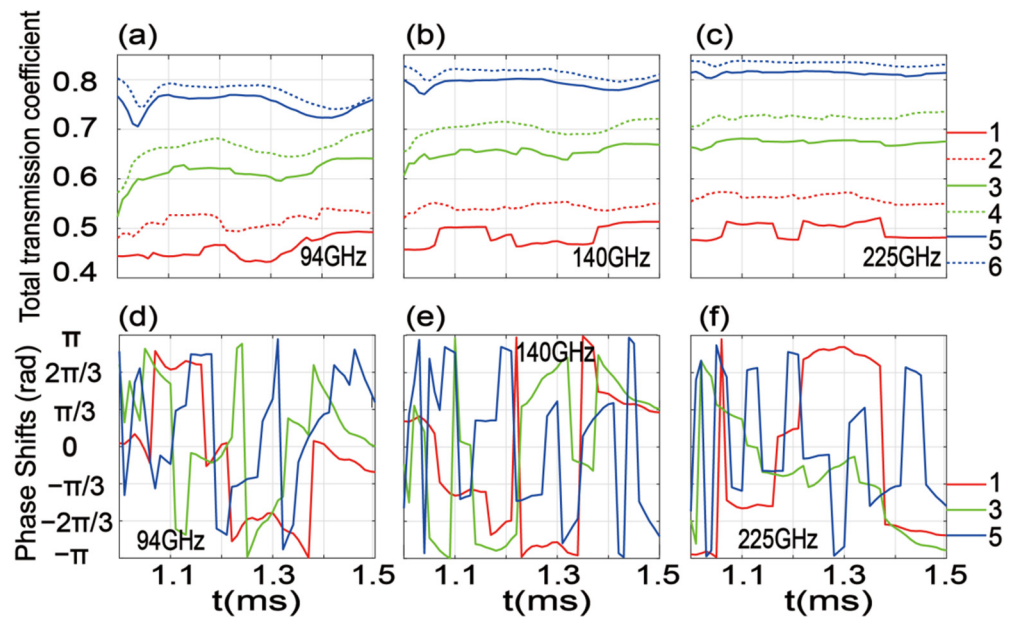


**Figure 2.** The time curves of the total transmission coefficients and phase shifts of the tail channels. (a–c) Total transmission coefficients of EHF signals with carrier frequencies of 94 GHz, 140 GHz, and 225 GHz, respectively; (d–f) Phase shifts of EHF signals with carrier frequencies of 94 GHz, 140 GHz, and 225 GHz, respectively.

In addition, as shown in Figure 2a–c, for a specific channel, the total transmission coefficient increases with the increases in carrier frequency. For instance, for channel 6, the transmission coefficient increases from about 0.78 at 94 GHz to about 0.84 at 225 GHz. Moreover, from Figure 2a–c, we can also find that the transmission coefficients of different combinations of carrier frequency and channel fluctuate with time, but that the fluctuation amplitude is small. Among them, the fluctuation amplitude of 3–6 channels at 94 GHz is the largest, reaching about 0.1, and the fluctuation amplitude of 5–6 channels at 225 GHz is the smallest, with only about 0.02. Overall, when 225 GHz carrier frequency and channel 6 (with a relatively large angle  $\alpha$ ) are selected, the maximum and most stable transmission coefficient performance can be obtained. In general, the total transmission coefficients always vary with time, and the total transmission coefficients for higher frequencies is generally higher than that of lower frequencies. The reason for this is that the plasma sheath is dispersive lossy media to EHF signals. For signals of normal incidence, the polarization loss is zero. Then, the absorption led by the collisions between free electrons and neutral particles becomes the main mechanism for the energy loss in EHF signals. The total absorption rate depends on the electron density, collision frequency, and the wave frequency [11]. High frequencies suffer less absorption than that of lower frequencies [24].

As shown in Figure 2d–f, different from the transmission coefficient, the phase shift fluctuates much more severely with time. The phase shift curve looks very messy, but it can still be seen that, for a specific carrier frequency, the fluctuation of phase shift is significantly more intense with an increase in angle  $\alpha$ . It should be noted that the phase shifts are measured in the range from  $-\pi$  to  $\pi$ , as it is not necessary to take the ambiguity

of whole cycles into account in the present modulation–demodulation problem. Once the phase varies from a value of smaller than  $\pi$  to greater than  $\pi$ , it would register as a sharp decrease in Figure 2, although it is still a continuous variation. The temporal variation of phase shift is led by the temporal variation of the wavelength in the plasma sheath. The plasma sheath is dispersive media, and its cutoff frequency is normally at the EHF band. According to geometrical optical theories, the refractive indices of plasma sheath for EHF waves are the functions of wave frequencies. In addition, the refractive indices are not close to 1, which is the refractive index of vacuum or neutral atmosphere. On the other hand, the wavelength is proportional to the refractive index. Thus, the EHF wavelength in the plasma sheath is obviously different from that in vacuum or neutral atmosphere. The refractive index depends on the electron density, electron collision frequency, and the wave frequency. In other words, the time-varying inhomogeneous plasma sheaths make the wavelength of propagating EHF signal vary in time during propagation. It should be noticed that the phase shifts are measured at a fix position in the present frame of reference. Hence, the varying wavelength makes the measured phase shifts vary with time.

The above results indicate that the total transmission coefficient and phase shift of the EHF communication in the plasma sheath wake region are very dependent on carrier frequency and channel angle  $\alpha$ , and that this dependence will affect the BER characteristics of EHF communication in the plasma sheath wake region, which are analyzed in detail in the next section.

### 3. Numerical Simulations on the BER

In this section, the time-varying BER characteristics of EHF signals in a plasma sheath with carrier frequencies of 94 GHz, 140 GHz, and 225 GHz and four modulation modes of 2ASK, 2PSK, 4QAM (QPSK), and 2FSK are studied by Monte Carlo simulation. Firstly, we randomly generate  $10^5$  digital signals and modulate them to the above three carrier frequencies using four different modulation modes. Then, the modulated signals are transmitted to the plasma sheath at the incident angle set in Section 2, and Gaussian white noise is added. Next, the modulated signals mixed with noise are demodulated. The plasma sheath causes signal attenuation and phase shift, resulting in bit errors in the received signal. Finally, the BER is statistically counted. Here, we take 2PSK modulation simulation system as an example to introduce the simulation process used. Assume that only one symbol duration is considered in 2PSK, and that the power of the signal transmitter is set to 1 mW. The carrier amplitude is set to  $\sqrt{0.002}$ . The 2PSK modulated signal can be expressed as Equation (5).

$$s_1 = \begin{cases} \sqrt{0.002}\cos\omega_c t \text{ send "1"} \\ -\sqrt{0.002}\cos\omega_c t \text{ send "0"} \end{cases} \quad (5)$$

Make the signal  $s_1$  pass through the plasma sheath module, Gaussian white noise module, and band-pass filter module in turn, and then obtain the signal  $s_2$  to be demodulated, which can be expressed as Equation (6).

$$s_2 = \begin{cases} a_1 \left( \sqrt{0.002}A\cos\omega_c t\cos\varphi + n(t) \right) \text{ send "1"} \\ a_1 \left( -\sqrt{0.002}A\cos\omega_c t\cos\varphi + n(t) \right) \text{ send "0"} \end{cases} \quad (6)$$

where  $A$  and  $\varphi$  are the total transmission coefficient and phase shift of the signal propagating in the plasma sheath, respectively,  $a_1$  represents the preliminary processing result of the phase shift caused by the sheath, and  $n(t)$  is a narrow-band Gaussian process which can be orthogonally decomposed.

$$a_1 = \begin{cases} 1 & |\varphi| \leq 90^\circ \\ -1 & |\varphi| > 90^\circ \end{cases} \quad (7)$$

$$n(t) = n_c(t)\cos\omega_c t - n_s(t)\sin\omega_c t \quad (8)$$

Finally, the signal  $s_2$  is coherently demodulated, and the output signal can be expressed as Equation (9).

$$s_3 = \begin{cases} a_1 \left( 0.001A \cos \varphi + \sqrt{0.0005} n_c(t) \right) \text{ send "1"} \\ a_1 \left( -0.001A \cos \varphi + \sqrt{0.0005} n_c(t) \right) \text{ send "0"} \end{cases} \quad (9)$$

where  $n_c(t)$  is the in-phase component of the narrowband white Gaussian noise output from the bandpass filter.

The BER of channels 3 and 6 are shown in Figure 3. The discontinuity in Figure 3 indicates that the BER is 0. Figure 3 shows that, under the same carrier frequency and noise level, the BER performance of channel 6 is better than that of channel 3, when 2ASK, 2PSK, and 4QAM (QPSK) are adopted. When 2FSK is adopted, the BER performance of channel 6 is better than that of channel 3 when the carrier center frequency is 94 GHz and 140 GHz, however the situation is just the opposite when the carrier center frequency is 225 GHz.

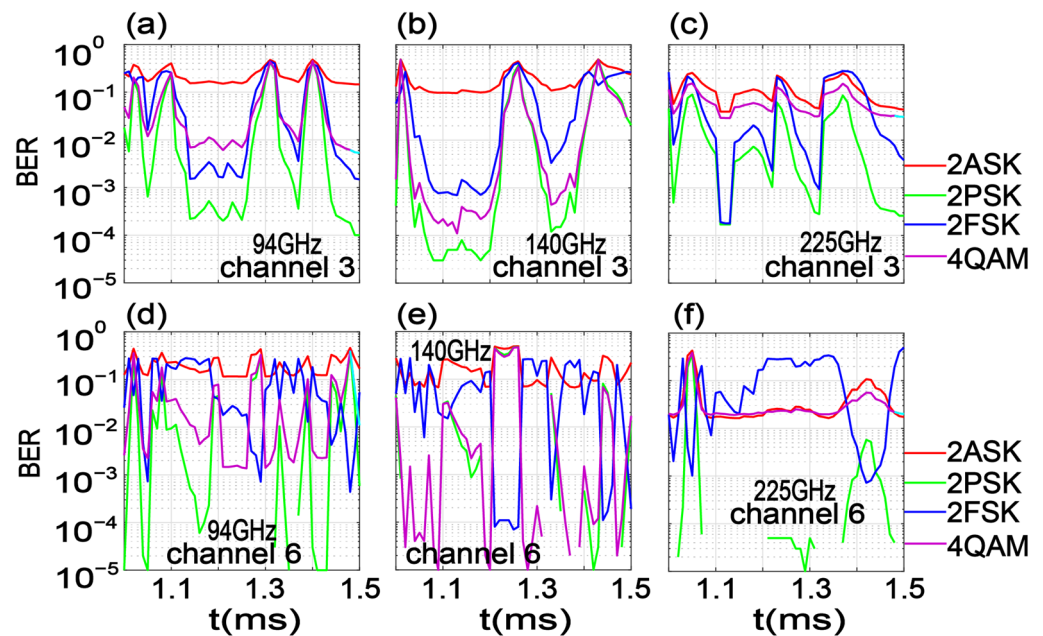


**Figure 3.** Under the same noise settings, BER performance of (a–c) channel 3 and (d–f) channel 6 when the carrier frequencies are 94 GHz (a,d), 140 GHz (b,e), and 225 GHz (c,f), respectively.

When 2ASK is adopted, the minimum BER magnitude is bigger than  $10^{-1}$  when the carrier frequency is 94 GHz, and between  $10^{-1}$  and  $10^{-2}$  when the carrier frequency is 140 GHz and 225 GHz. Under the same noise level, the BER performance improves with an increase in carrier frequency. When channel 6 and 225 GHz carrier frequency are selected, BER can reach optimum performance.

When 2PSK is adopted, in channel 3, the minimum BER magnitude is between  $10^{-3}$  and  $10^{-4}$  when the carrier frequency is 94 GHz and 225 GHz, and between  $10^{-4}$  and  $10^{-5}$  when the carrier frequency is 140 GHz. The BER of channel 6 can reach zero at all three carrier frequencies, but the BER remains zero for a longer time when the carrier frequencies are 140 GHz and 225 GHz. The BER performance is better when channel 6 is adopted and with a carrier frequency of 140 GHz and 225 GHz.

When 2FSK is adopted, in channel 3, the minimum BER magnitude is between  $10^{-2}$  and  $10^{-3}$  when the carrier center frequency is 94 GHz, and between  $10^{-3}$  and  $10^{-4}$  when the carrier center frequency is 140 GHz and 225 GHz. In channel 6, the minimum BER magnitude is between  $10^{-3}$  and  $10^{-4}$  when the carrier center frequency is 94 GHz and 225 GHz, and between  $10^{-4}$  and  $10^{-5}$  when the carrier center frequency is 140 GHz. When channel 6 and a 140 GHz carrier center frequency are selected, the BER performance is the

best. Under the same channel and noise level, the BER performance of 2FSK is better than 2ASK, but worse than 2PSK.

When using 4QAM (QPSK), the minimum BER magnitude is between  $10^{-2}$  and  $10^{-3}$  when the carrier frequency is 94 GHz, and between  $10^{-1}$  and  $10^{-2}$  when the carrier frequency is 225 GHz. When the carrier frequency is 140 GHz, the minimum BER magnitude is between  $10^{-3}$  and  $10^{-4}$  in channel 3, and zero in channel 6. The BER performance is the best when channel 6 and a 140 GHz carrier frequency are selected.

In summary, when 2PSK modulation with a carrier frequency of 140 GHz or 225 GHz, or 4QAM (QPSK) modulation with a carrier frequency of 140 GHz is adopted, better BER performance can be obtained from channel 6.

#### 4. Discussion

Previous studies have mostly focused on the communication “blackout” on the wall or the nose of the vehicle. Only a few studies have analyzed the tail communication performance, mainly for Ka band, and the plasma sheath parameters were simply set (e.g., only typical values of electron density at certain heights were used) [36–38]. Moreover, when the electron density of the plasma sheath reaches about  $10^{20} \text{ m}^{-3}$ , the Ka band signal cannot penetrate the plasma sheath. Based on the dynamic time-varying plasma sheath model, the communication performance of EHF signals in the tail channels of the reentry vehicle is investigated for the first time in this study. Our results indicate that, when an EHF band is adopted in the tail of the plasma sheath and the electron density is in the magnitude of  $10^{19} \text{ m}^{-3}$ , the transmission coefficient can be greater than 0.7, even if the carrier frequency is 94 GHz.

It can be seen from Section 2 that the transmission coefficient increases and the phase shift fluctuates more violently as angle  $\alpha$  increases. As is illustrated in Section 3, when 2PSK modulation with a carrier frequency of 140 GHz or 225 GHz, or 4QAM (QPSK) modulation with a carrier frequency of 140 GHz, and channel 6 are adopted, better BER performance can be obtained.

Figure 4 illustrates the BER variation with the threshold of the 2ASK and 2PSK systems, the schematic diagram of 2FSK non-coherent demodulation, and its waveforms of the nodes. As can be seen from Figure 4a, the optimal threshold of the 2PSK system is 0, which is independent of amplitude, while the optimal threshold of the 2ASK system is half of amplitude, which is closely related to amplitude. In addition, the demodulation method of the 4QAM (QPSK) system is similar to that of 2PSK, and the threshold is also 0, which is independent of amplitude. As can be seen from Figure 4b,c, the 2FSK communication system does not need to set the decision threshold artificially, as it makes a decision based on the size of the two quadrature demodulation signals. The bandwidth of 2ASK, 2PSK, and 4QAM (QPSK) modulation systems is twice the symbol rate, while the bandwidth of 2FSK is the absolute value of the difference between the two carrier frequencies plus twice the symbol rate. The frequency band utilization of a communication system is defined as the amount of information transmitted on a unit frequency band per second. The bandwidth utilization of 2ASK and 2PSK is 0.5 bit/s/Hz, and that of 4QAM (QPSK) is 1 bit/s/Hz, while that of 2FSK is less than 0.5 bit/s/Hz). Therefore, for the four modulations involved in this article, 4QAM (QPSK) has the highest bandwidth utilization, while 2FSK has the lowest bandwidth utilization. Based on the above analysis, it can be concluded that the 2PSK system can be selected if the anti-noise performance of the system is considered first, while the 4QAM (QPSK) system can be selected if the bandwidth utilization is considered first.

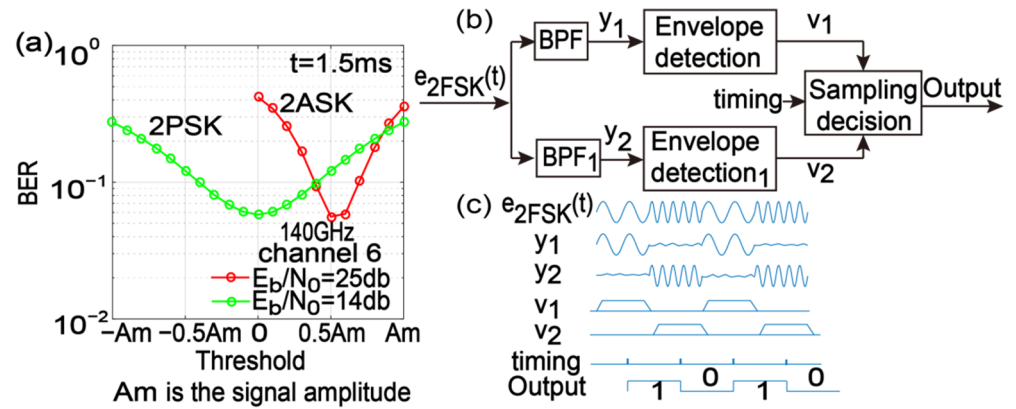


Figure 4. (a) The change of BER with the threshold, (b) schematic diagram of 2FSK non-coherent demodulation, (c) the waveforms of the nodes in the schematic diagram of 2FSK non-coherent demodulation.

In addition, the BER is also closely related to the channel electron density level and channel length. Better BER performance in channel 6 may be controlled by these two factors. Here, we further analyze the maximum electron density and channel length of all channels at some selected moments, and the results are illustrated in Figure 5. According to Figure 5, the maximum electron density decreases with an increase in  $\alpha$  after 1.2 ms. Generally, in the early stage of sheath evolution (before 1.2 ms), compared with the fluctuation of electron density of channels with  $\alpha < 60^\circ$ , the fluctuation of electron density of channels with  $\alpha \geq 60^\circ$  is more serious, and the lengths of channels with  $\alpha \geq 60^\circ$  are very long. When  $2^\circ \leq \alpha \leq 50^\circ$ , the maximum electron density is relatively larger and may result in worse BER performance, even if the length of the channel is small. When  $50^\circ < \alpha \leq 60^\circ$ , both of the maximum electron density and the channel length are relatively small, which may make it easier to obtain better BER performance.

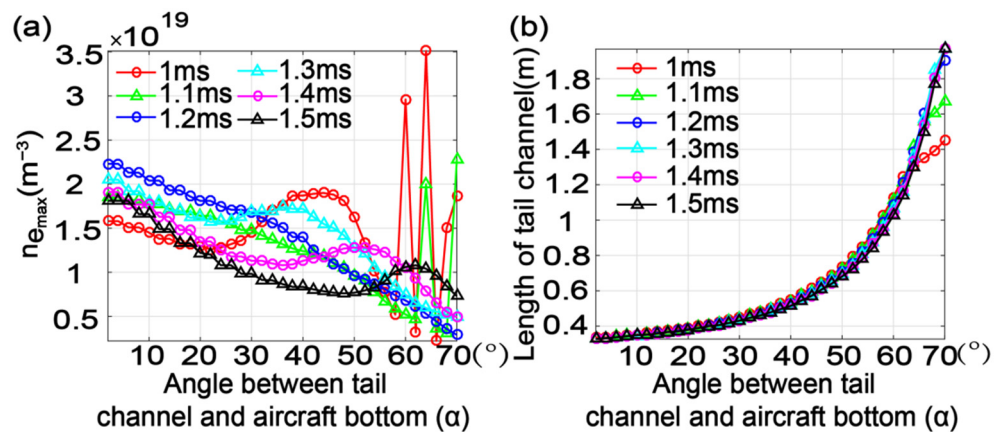


Figure 5. (a) The maximum electron density of different tail channels at a specific time, (b) the channel length of different tail channels at a specific time.

### 5. Conclusions

This article studied the total transmission coefficient and phase shift characteristics of EHF signals in the tail channels of a hypersonic vehicle. In addition, the BER characteristics of EHF signals with different modulation in the tail channels are analyzed. The results indicate that the total transmission coefficient and phase shift are directly affected by channel and carrier frequency. Generally speaking, as the angle between the tail channel and the tail of the vehicle increases, the attenuation of the EHF signals in the tail channel decreases and the phase shift fluctuates more drastically. By comparing the BER characteristics of

EHF signals modulated by 2ASK, 2PSK, 4QAM (QPSK), and 2FSK in tail channels, it is found that, when the communication system served a hypersonic vehicle that selected 2PSK modulation with a carrier frequency of 140 GHz or 225 GHz, or 4QAM (QPSK) modulation with a carrier frequency of 140 GHz, and the tail channel with an angle between 50° and 60° to the tail of the vehicle, better communication BER performance can be achieved. This is the first result of the communication performance analysis of EHF signals with different modulation modes in different channels at the tail of the vehicle, which is helpful in solving the “blackout” problem when relay communication is adopted in engineering. Nevertheless, a multipath effect may exist in the wake region communication process, because the wake region is much larger than the aft region. The influence of multipath on the BER characteristics of EHF signals needs to be further studied.

**Author Contributions:** Conceptualization, Y.W. and K.Y.; methodology, K.Y. and X.Y.; software, X.Y. and J.X.; validation, X.Y. and Y.L.; formal analysis, X.Y.; investigation, X.Y. and K.Y.; resources, Y.W.; data curation, Y.W.; writing—original draft preparation, X.Y. and K.Y.; writing—review and editing, Y.W. and Y.L.; visualization, X.Y. and J.X.; supervision, Y.W. and K.Y.; project administration, K.Y. and Y.L.; funding acquisition, Y.W. All authors have read and agreed to the published version of the manuscript.

**Funding:** This work was supported by the National Natural Science Foundation of China under Grant No. 61861031.

**Institutional Review Board Statement:** Not applicable.

**Informed Consent Statement:** Not applicable.

**Data Availability Statement:** Not applicable.

**Conflicts of Interest:** The authors declare no conflict of interest.

## Abbreviations

EHF	Extremely High Frequency
BER	Bit Error Rate
RAM C-I	Radio Attenuation Measurements C-I
RAM C-II	Radio Attenuation Measurements C-II
TDRS	NASA’s Tracking and Data Relay Satellite

## References

- Schouler, M.; Préveraud, Y.; Mieussens, L. Survey of flight and numerical data of hypersonic rarefied flows encountered in earth orbit and atmospheric reentry. *Prog. Aerosp. Sci.* **2020**, *118*, 100638. [\[CrossRef\]](#)
- Starkey, R.P. Hypersonic Vehicle Telemetry Blackout Analysis. *J. Spacecr. Rocket.* **2015**, *52*, 426–438. [\[CrossRef\]](#)
- Gillman, E.D.; Foster, J.E.; Blankson, I.M. *Review of Leading Approaches for Mitigating Hypersonic Vehicle Communications Blackout and a Method of Ceramic Particulate Injection via Cathode Spot Arcs for Blackout Mitigation*; NASA/TM-2010-216220; NASA: Washington, DC, USA, 2010.
- Savino, R.; D’elia, M.E.; Carandente, V. Plasma Effect on Radiofrequency Communications for Lifting Reentry Vehicles. *J. Spacecr. Rocket.* **2015**, *52*, 417–425. [\[CrossRef\]](#)
- Hartunian, R.; Stewart, G.; Ferguson, S.; Curtiss, T.; Seibold, R. *Causes and Mitigation of Radio Frequency (RF) Blackout During Reentry of Reusable Launch Vehicles*; Technical Report; Aerospace Corporation: Segundo, CA, USA, 2007.
- Belov, I.F.; Borovoy, V.Y.; Gorelov, V.A.; Kireev, A.Y.; Korolev, A.S.; Stepanov, E.A. Investigation of Remote Antenna Assembly for Radio Communication with Reentry Vehicle. *J. Spacecr. Rocket.* **2001**, *38*, 249–256. [\[CrossRef\]](#)
- Song, L.; Li, X.; Bai, B.; Liu, Y. Effects of Plasma Sheath on the Signal Detection of Narrowband Receiver. *IEEE Trans. Plasma Sci.* **2018**, *47*, 251–258. [\[CrossRef\]](#)
- Zhang, Y.; Liu, Y.; Li, X. Total-Field/Scattered-Field Formulation for FDTD Analysis of Plane-Wave Propagation through Cold Magnetized Plasma Sheath. *IEEE Trans. Antennas Propag.* **2019**, *68*, 377–387. [\[CrossRef\]](#)
- Cianca, E.; Rossi, T.; Yahalom, A.; Pinhasi, Y.; Farserotu, J.; Sacchi, C. EHF for Satellite Communications: The New Broadband Frontier. *Proc. IEEE* **2011**, *99*, 1858–1881. [\[CrossRef\]](#)
- Viti, L.; Hu, J.; Coquillat, D.; Politano, A.; Knap, W.; Vitiello, M.S. Efficient Terahertz detection in black-phosphorus nano-transistors with selective and controllable plasma-wave, bolometric and thermoelectric response. *Sci. Rep.* **2016**, *6*, 20474. [\[CrossRef\]](#)

11. Chen, J.; Yuan, K.; Shen, L.; Deng, X.; Hong, L.; Yao, M. Studies of terahertz wave propagation in realistic reentry plasma sheath. *Prog. Electromagn. Res.* **2016**, *157*, 21–29. [[CrossRef](#)]
12. Zheng, L.; Zhao, Q.; Liu, S.; Ma, P.; Huang, C.; Tang, Y.; Chen, X.; Xing, X.; Zhang, C.; Luo, X. Theoretical and experimental studies of 35 GHz and 96 GHz electromagnetic wave propagation in plasma. *Prog. Electromagn. Res.* **2012**, *24*, 179–192. [[CrossRef](#)]
13. Yuan, K.; Chen, J.; Shen, L.; Deng, X.; Yao, M.; Hong, L. Impact of Reentry Speed on the Transmission of Obliquely Incident THz Waves in Realistic Plasma Sheaths. *IEEE Trans. Plasma Sci.* **2018**, *46*, 373–378. [[CrossRef](#)]
14. Guo, L.; Guo, L.; Li, J. Propagation of terahertz electromagnetic waves in a magnetized plasma with inhomogeneous electron density and collision frequency. *Phys. Plasmas* **2017**, *24*, 022108. [[CrossRef](#)]
15. Li, S.; Li, J.; Zhu, Z.; Cui, W. The effect of ions on terahertz wave propagation characteristics in plasma sheath. In Proceedings of the 2014 12th International Conference on Signal Processing (ICSP), Hangzhou, China, 19–23 October 2014; pp. 2398–2402.
16. Yuan, C.-X.; Zhou, Z.-X.; Xiang, X.-L. Properties of Terahertz Waves Propagation in a Bounded Plasma Slab with High Collision Frequency and High Density. In Proceedings of the 2010 International Conference on Optoelectronics and Image Processing, Haikou, China, 11–12 November 2010; Volume 2, pp. 135–140.
17. Zheng, L.; Zhao, Q.; Liu, S.; Xing, X.; Chen, Y. Theoretical and experimental studies of terahertz wave propagation in unmagnetized plasma. *J. Infrared Millim. Terahertz Waves* **2014**, *35*, 187–197. [[CrossRef](#)]
18. Yuan, C.-X.; Zhou, Z.-X.; Zhang, J.W.; Xiang, X.-L.; Yue, F.; Sun, H.-G. FDTD Analysis of Terahertz Wave Propagation in a High-Temperature Unmagnetized Plasma Slab. *IEEE Trans. Plasma Sci.* **2011**, *39*, 1577–1584. [[CrossRef](#)]
19. Tang, R.; Xiong, Z.; Yuan, K.; Mao, M.; Wang, Y.; Deng, X. EHF Wave Propagation in the Plasma Sheath Enveloping Sharp-Coned Hypersonic Vehicle. *IEEE Antennas Wirel. Propag. Lett.* **2021**, *20*, 978–982. [[CrossRef](#)]
20. He, G.; Zhan, Y.; Ge, N.; Pei, Y.; Wu, B. Measuring the Time-Varying Channel Characteristics of the Plasma Sheath from the Reflected Signal. *IEEE Trans. Plasma Sci.* **2014**, *42*, 3975–3981. [[CrossRef](#)]
21. Zhang, J.; He, G.; Bai, P.; Ge, N. Dynamic channel modeling for communication through turbulent plasma sheath. In Proceedings of the 2015 International Conference on Wireless Communications & Signal Processing (WCSP), Nanjing, China, 15–17 October 2015; pp. 1–5.
22. Frankel, D.S.; Nebolsine, P.E.; Miller, M.G.; Glynn, J.M. Re-entry plasma induced pseudorange and attenuation effects in a GPS simulator. *Def. Secur.* **2004**, *5420*, 65–74. [[CrossRef](#)]
23. Ohler, S.G.; Gilchrist, B.E.; Gallimore, A.D. Electromagnetic signal modification in a localized high-speed plasma flow: Simulations and experimental validation of a stationary plasma thruster. *IEEE Trans. Plasma Sci.* **1999**, *27*, 587–594. [[CrossRef](#)]
24. Ouyang, W.; Jin, T.; Wu, Z.; Deng, W. Study of Terahertz Wave Propagation in Realistic Plasma Sheath for the Whole Reentry Process. *IEEE Trans. Plasma Sci.* **2021**, *49*, 460–465. [[CrossRef](#)]
25. Van der Vleuten, E.; Lagendijk, V. Transnational infrastructure vulnerability: The historical shaping of the 2006 European 221 “Blackout”. *Energy Policy* **2010**, *38*, 2042–2052. [[CrossRef](#)]
26. Savajano, R.; Potter, D.F.; Joshi, O.; Leyland, P. Radiation Analysis for Two Trajectory Points of the Fire II Entry. *Int. J. Aerosp. Eng.* **2012**, 1–9. [[CrossRef](#)]
27. Lin, T.; Sproul, L. Influence of reentry turbulent plasma fluctuation on EM wave propagation. *Comput. Fluids* **2006**, *35*, 703–711. [[CrossRef](#)]
28. Clarey, M.P.; Greendyke, R.B. Three-Temperature Thermochemical Nonequilibrium Model with Application to Slender-Body Wakes. *J. Thermophys. Heat Transf.* **2019**, *33*, 721–737. [[CrossRef](#)]
29. Yamagishi, M.; Yahagi, Y.; Ota, M.; Hirose, Y.; Udagawa, S.; Inage, T.; Kubota, S.; Fujita, K.; Ohtani, K.; Nagai, H. Quantitative density measurement of wake region behind reentry capsule (Improvements in accuracy of 3D reconstruction by evaluating the view-angle of measurement system). *J. Fluid Sci. Technol.* **2021**, *16*, JFST0021. [[CrossRef](#)]
30. Jung, M.; Kihara, H.; Abe, K.I.; Takahashi, Y. Numerical simulation of plasma flows and radio-frequency blackout in atmospheric reentry demonstrator mission. In Proceedings of the 47th AIAA Fluid Dynamics Conference, Denver, CO, USA, 5–9 June 2017.
31. Kim, M.; Keidar, M.; Boyd, I. Two-dimensional Model of an Electromagnetic Layer for the Mitigation of Communications Blackout. In Proceedings of the 47th AIAA Aerospace Sciences Meeting including The New Horizons Forum and Aerospace Exposition, Orlando, FL, USA, 5–8 January 2009.
32. Takahashi, Y.; Nakasato, R.; Oshima, N. Analysis of Radio Frequency Blackout for a Blunt-Body Capsule in Atmospheric Reentry Missions. *Aerospace* **2016**, *3*, 2. [[CrossRef](#)]
33. Paulat, J.; Boukhobza, P. *Re-Entry Flight Experiments Lessons Learned—The Atmospheric Reentry Demonstrator ARD; Flight Experiments for Hypersonic Vehicle Development*, NATO Research and Technology Organization RTO-EN-AVT-130; RTO: Neuilly-sur-Seine, France, 2007; pp. 1–46.
34. Fan, J.; Zhang, Y.; Jiang, J. Monte Carlo modeling of electron density in hypersonic rarefied gas flows. *AIP Conf. Proc.* **2014**, *1628*, 148–154. [[CrossRef](#)]
35. Hu, B.J.; Wei, G.; Lai, S.L. SMM analysis of reflection, absorption, and transmission from nonuniform magnetized plasma slab. *IEEE Trans. Plasma Sci.* **1999**, *27*, 1131–1136. [[CrossRef](#)]
36. Li, Y.; Luo, B.; Guo, W. Feasibility Analysis of Using Ka-Band of TRDS to support Wireless Communication for spacecraft Reentry. *Manned Spacefl.* **2015**, *21*, 582–588.

- 
37. Wang, J.; Jing, Y.; Yang, X. On Approaches to Overcome Spacecraft Reentry Communication Blackout Using Satellite Relay. *Spacecr. Eng.* **2015**, *24*, 1–8.
  38. Wen, Z.; Chen, C.; Ling, Y.; Zhou, T. A Research on Communications Blackout Problem in Ka-Band by Relay Method. *J. Air Force Eng. Univ. Nat. Sci. Ed.* **2016**, *17*, 18–22.